ISSN 0965-5441, Petroleum Chemistry, 2020, Vol. 60, No. 4, pp. 516–524. © Pleiades Publishing, Ltd., 2020.
Russian Text © The Author(s), 2020, published in Sovremennye Molekulyarnye Sita, 2020.

Acetone Conversion to Isobutylene over Magnesium-Containing Micro-Mesoporous MOR Zeolites

O. A. Ponomareva[a, b], A. A. Maltseva[a], A. G. Popov[a], I. V. Dobryakova[a], I. A. Kasyanov[a, *], and I. I. Ivanova[a, b]

[a] *Faculty of Chemistry, Moscow State University, Moscow, 119991 Russia*
[b] *Topchiev Institute of Petrochemical Synthesis, Russian Academy of Sciences, Moscow, 119991 Russia*
**e-mail: i.a.kasyanov@gmail.com*

Received November 14, 2019; revised December 4, 2019; accepted December 10, 2019

Abstract—Isobutylene synthesis from acetone in the presence of micro–mesoporous MOR zeolites obtained by hydrothermal recrystallization and modified with magnesium acetate by incipient wetness impregnation has been studied. A kinetic study of the reaction has been conducted, and product formation routes have been determined. It has been found that an increase in the mesopore content leads to an increase in the catalyst activity owing to the removal of diffusion restrictions. It has been shown that isobutylene formation occurs on both Lewis and Brønsted acid sites. The modification of the initial aluminosilicates with magnesium has been found to decrease the number and strength of Brønsted acid sites and thereby lead to a decrease in the number of side reactions and an increase in the time-on-stream stability of the catalysts.

Keywords: acetone, isobutylene, micro–mesoporous catalysts, recrystallization, acid sites, modification, magnesium, mordenite

DOI: 10.1134/S0965544120040118

Against the background of ever-increasing crude oil prices, the development of methods for synthesizing high-demand chemicals from renewable raw materials is promising. One of these methods is isobutylene synthesis from acetone that is a product of biomass fermentation or pyrolysis and bioethanol steam reforming and a byproduct of propylene oxide synthesis and cumene production in phenol synthesis [1, 2]. Isobutylene as a monomer is commonly used in the synthesis of butyl rubber and polyisobutylene and in the production of methyl methacrylate and methyl *tert*-butyl ether.

Acetone conversion to isobutylene was studied in the presence of zeolite catalysts of various framework types (BEA [1–6], MFI [2, 4, 6–12], FER [6], TON [6], FAU (Y, X) [13], MOR [14]), molecular sieves (SAPO-34 [15], MCM-41 [6, 16]), oxide catalysts supported on silica gel (WO_3/SiO_2 [17], Al_2O_3/SiO_2 [18]), and mixed oxides $Zn_xZr_yO_z$ [19–21].

Acetone conversion to isobutylene is a complex process, which includes ketonization, aldol condensation, dehydration, cyclization, cracking, isomerization, aromatization, and other reactions [1, 21], which lead to the formation of a large set of products. It was shown [2, 6] that strong acid sites contribute to the occurrence of side reactions and the formation of condensation products. Although there is still no complete clarity concerning the nature of isobutylene selective sites, most researchers believe that these sites are of medium strength [1, 2, 6, 14, 20–22]. In this context, it is of interest to use magnesium as a modifier, because it is known that the introduction of magnesium leads to a decrease in the number of strong Brønsted acid sites and an increase in the number of Lewis acid sites [23–25]. It was previously shown that promising heterogeneous catalysts for acetone conversion to isobutylene are micro–mesoporous molecular sieves, which combine high acidity and unique molecular stereoselectivity of zeolites with the transport characteristics of mesoporous materials; it was found that an increase in the mesopore content in the catalyst leads to an increase in the initial rates of acetone conversion and isobutylene formation owing to the removal of diffusion restrictions [14].

Therefore, in this study, acetone conversion to isobutylene in the presence of Mg-containing micro–mesoporous catalysts synthesized by mordenite (MOR) recrystallization [26] and having different amounts of mesopores has been first analyzed, a kinetic study of the reaction has been conducted, the sequence of formation of reaction products has been found, and the effect of the pore characteristics of the catalyst and magnesium modification on the physicochemical and catalytic properties has been studied.

EXPERIMENTAL

Mordenite with a silica ratio of $SiO_2/Al_2O_3 = 97$ (Zeolyst, product name CBV 90A) was used. Micro–mesoporous zeolites (RM) based on MOR were synthesized by the recrystallization procedure described in [27]. The degree of recrystallization was varied by changing the alkali concentration. To provide the formation of RM-1, RM-2, and RM-3 materials with different amounts of micro- and mesopores, alkali/zeolite ratios of 3, 5, and 10 mmol(NaOH)/g(MOR), respectively, were used.

Magnesium modification of the catalysts was conducted by incipient wetness impregnation with a magnesium acetate solution to provide the metal content in the sample of 3 wt %. After preparation, all samples were calcined at 550°C in an air stream for 24 h.

The chemical composition of the samples was determined by X-ray fluorescence analysis on a Thermo Scientific ARL Perform'X instrument equipped with a 3.5-kW rhodium tube.

X-ray diffraction (XRD) patterns were recorded on a Bruker D2 PHASER diffractometer (CuK_α radiation) in an angular range of $5° < 2\theta < 50°$. Small-angle X-ray scattering (SAXS) patterns were recorded in the angular range of $1.5° < 2\theta < 5°$. The diffraction patterns were processed using the Bruker DIFFRAC.EVA software package. Phases were identified in accordance with the ICDD PDF2 database.

Electron microscope images of the samples were recorded on a JEOL JEM 2010 transmission electron microscope using a 200-keV electron beam.

The pore structure characteristics of the zeolites were studied on a Micromeritics ASAP 2000 automatic porosimeter. Micropore volume was determined by the t-plot method. The pore volume taking into account adsorption in micropores and mesopores and on the outer surface was calculated from the amount of nitrogen sorbed at a relative pressure of $P/P_0 = 0.95$. Mesopore volume was determined from the difference between the total pore volume and the micropore volume.

The acidic properties of the samples were studied by temperature-programmed desorption of ammonia (NH_3 TPD) on a USGA-101 universal sorption gas analyzer as described in [14] and by infrared (IR) spectroscopy of adsorbed pyridine (Py). Infrared spectra were recorded on a Nicolet Protégé 460 Fourier transform spectrometer equipped with an MCT detector with an optical resolution of 4 cm^{-1} in a range of 4000–400 cm^{-1}. The catalysts were activated in an IR cell at 400°C and a pressure of 10^{-5} torr for 2 h. Pyridine adsorption was run at 150°C for 30 min; it was followed by evacuation at 150°C for 15 min. The recorded IR spectra were processed using the OMNIC ESP software package (version 7.3); the attribution of bands in the IR spectra was conducted using data of [28].

Catalytic tests were conducted in a fixed-bed flow reactor at atmospheric pressure, a temperature of 500°C, and a feed space velocity of 2–72 g/(g h), while diluting the reaction mixture with nitrogen (20 mL/min). The chromatographic analysis of the liquid and gaseous reaction products was conducted on a Kristall 2000M gas–liquid chromatograph (Chromatec Analytic) equipped with a flame ionization detector and a capillary column coated with the SE-30 phase using nitrogen as the carrier gas. Methanol was used as an internal standard for liquid samples. To determine the amount of CO_2 and separate C_1–C_2 light hydrocarbons (HCs), gaseous samples were also analyzed on a Kristall 2000M chromatograph equipped with a thermal conductivity detector and a packed column coated with the Porapak Q phase using hydrogen as the carrier gas. The products were identified using individual organic substances and by the gas chromatography–mass spectrometry method on a Thermo Trace GC Ultra chromatograph and a Thermo DSQ II mass spectrometer using a 50-m long quartz capillary column with the Ultra 1 nonpolar liquid phase. The catalytic properties of the samples were characterized according to acetone conversion and product selectivity. Initial reaction rate was determined by differentiating the initial portions of the rate curves characterizing the dependence of the reactant conversion on the contact time.

Ethanol conversion and target product selectivities and yields were calculated using the chromatographic analysis results.

Ethanol conversion (K) and ith product molar selectivity (S_i) were calculated by the following formulas:

$$K = 100 \times (k_i Q_i r_i / M_i) / (S(k_i Q_i r_i / M_i) + k_{\text{acetone}} Q_{\text{acetone}} / M_{\text{acetone}}),\ \%,$$

$$S_i = 100 \times (k_i Q_i / M_i) / S(k_i Q_i / M_i),\ \%,$$

where Q_i is the area of the chromatographic peak of the ith product, k_i is the coefficient of concordance between the peak area and the weight fraction of the product, M_i is the molecular weight of the ith product, and r_i is the coefficient taking into account the number of acetone molecules included in the ith product. Calibration coefficients for acetone, mesityl oxide, and acetic acid were determined by the absolute calibration method; reference values were taken for the other substances.

The ith product yield (Y_i) was calculated as follows:

$$Y_i = KS_i/100,\ \%.$$

Table 1. Physicochemical properties of the samples

Sample	V_{total}, cm^3/g	V_{micro}, cm^3/g	V_{micro}/V_{total}	SiO_2/Al_2O_3	a_0, μmol NH_3/g	a_0, μmol Al/g
MOR	0.24	0.16	0.66	97	436	1.3
MgMOR	0.24	0.16	0.66	96	863	2.6
RM-1	0.34	0.13	0.38	92	376	1.3
MgRM-1	0.27	0.11	0.41	–	782	2.3
RM-2	0.45	0.09	0.2	94	319	0.9
MgRM-2	0.40	0.05	0.13	–	725	2.1
RM-3	0.80	0.03	0.04	96	276	0.8
MgRM-3	0.68	0	0	–	394	1.2

RESULTS AND DISCUSSION

Physicochemical Properties of the Catalysts

The physicochemical properties of the initial, Mg-containing, and recrystallized samples are shown in Table 1.

It is evident that the original MOR and micro–mesoporous samples have an identical chemical composition; that is, during recrystallization, the partially dissolved zeolite is completely incorporated into the structure of the synthesized material.

According to XRD, SAXS, low-temperature nitrogen adsorption, and transmission electron microscopy data, the synthesized micro–mesoporous materials with different degrees of recrystallization are similar to materials described in [26] (not shown in this manuscript) and are as follows: mesoporous zeolite crystals coated with a mesoporous layer (RM-1), zeolite/MCM-41 micro–mesoporous nanocomposites (RM-2), and a mesoporous material with zeolite fragments incorporated into the walls (RM-3). Magnesium modification does not lead to a significant change in the pore characteristics of the samples (Table 1).

The study of the acidic properties of the catalysts consisted in the determination of the amount, strength, and nature of acid sites by NH_3 TPD and IR spectroscopy of adsorbed Py molecules.

Figure 1 shows NH_3-TPD curves for the micro–mesoporous samples with and without magnesium. According to NH_3 TPD, the desorption curve of the original MOR sample has almost the same shape as that of the curve for RM-1 and exhibits two peaks with maxima at 170 and 460°C; the first maximum corresponds to weak acid sites and physically adsorbed ammonia molecules, while the second maximum corresponds to strong acid sites. An increase in the degree of recrystallization leads to a shift of the high-temperature maximum to the region of lower temperatures, which indicates a decrease in the strength of the acid sites and the total number of acid sites (Table 1). Differences in the number of acid sites in the micro–mesoporous materials at an identical Si/Al ratio can be attributed to the fact that during the formation of the mesoporous phase, a portion of aluminum is incorporated into the walls of the material and becomes inaccessible to ammonia molecules. This assumption is supported by the fact that the calculated ratio of the amount of ammonia desorbed from the samples to the amount of aluminum in them decreases upon switching from MOR to RM-3 (Table 1).

Magnesium modification leads to an increase in the total acidity; in addition, the maximum of the

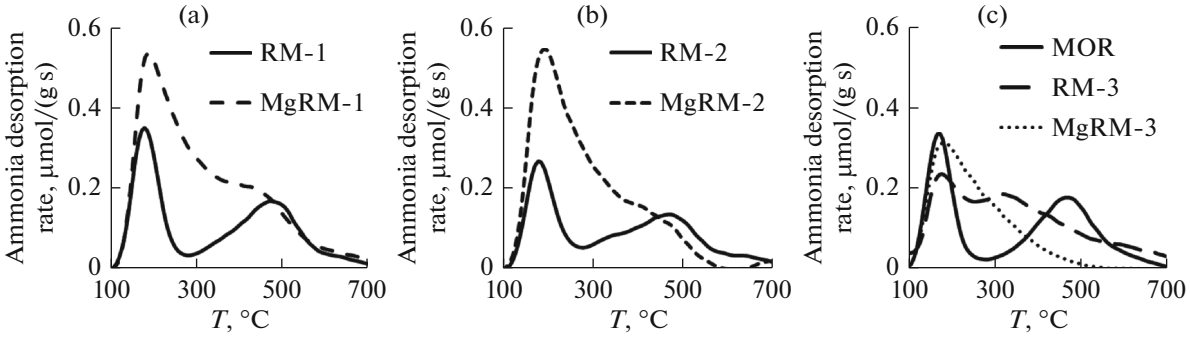

Fig. 1. Ammonia TPD curves for (a) the RM-1 and MgRM-1; (b) RM-2 and MgRM-2; and (c) MOR, RM-3, and MgRM-3 samples.

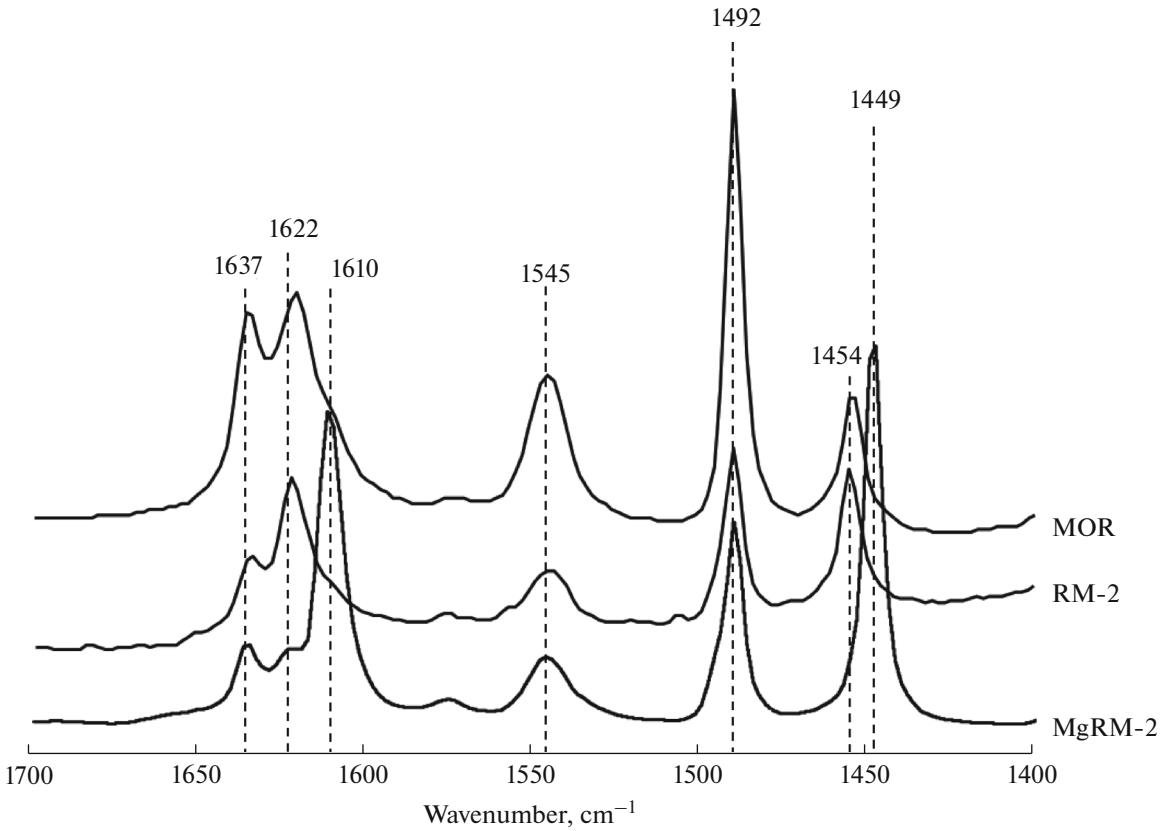

Fig. 2. Infrared spectra of Py adsorbed on the MOR, RM-2, and MgRM-2 samples.

high-temperature peak of ammonia desorption is shifted to the region of lower temperatures; in the case of the MgRM-3 sample, the maximum is not observed. Thus, the magnesium-containing samples mostly contain weak and medium-strength acid sites.

The nature of acid sites was determined using the IR spectra of adsorbed Py, which indicate the presence of the Brønsted (1545, 1637 cm^{-1}) and Lewis acid sites (1454, 1622 cm^{-1}) in the initial MOR and recrystallized samples (Fig. 2). The spectrum of Py adsorbed on the RM-1 sample did not differ from the spectrum recorded for the original MOR sample. With an increase in the degree of recrystallization, the total number of acid sites decreases, while the amount of Lewis acid sites increases. Apparently, in this case, the presence of Lewis acid sites is attributed to a partial scission of the Si–O–Al bonds.

Magnesium modification leads to a decrease in the intensity of the band corresponding to Brønsted acid sites (1637, 1545 cm^{-1}); however, in this case, new bands at 1610 and 1449 cm^{-1} appear; they are attributed to Lewis acid sites (Fig. 2). The authors of [25] believe that, during modification with magnesium (3 wt %), the added Mg^{2+} ion interacts with the protons of bridged hydroxyls to form $Mg(OH)^+$; therefore, the number of Lewis acid sites increases, and the number of Brønsted acid sites decreases.

Catalytic Properties

The catalytic conversion of acetone is a complex multi-route process; the reaction products contain, in addition to the target product (isobutylene), methane, C_2–C_4 light HCs, C_5–C_7 olefins, C_7–C_{10} aromatic HCs, acetic acid, mesityl oxide, and carbon dioxide.

To control the isobutylene selectivity, a kinetic study of the reaction was conducted to determine the acetone conversion scheme. The kinetic study of acetone conversion to isobutylene was conducted in the presence of MgRM-2 at 500°C in a broad contact time range of 0.014–0.5 h. The determined dependences of yields of all reaction products on the feedstock conversion at varying contact time are shown in Fig. 3. The curves for primary products have a nonzero tangent slope in the region of low conversions. Unstable products are characterized by a curve passing through a maximum. Based on the data, the reaction products were classified (Table 2) and an acetone conversion scheme was proposed (Fig. 4).

It is known from the literature [7, 16, 22] that the catalytic conversion of acetone occurs through aldol condensation to form diacetone alcohol; however, it

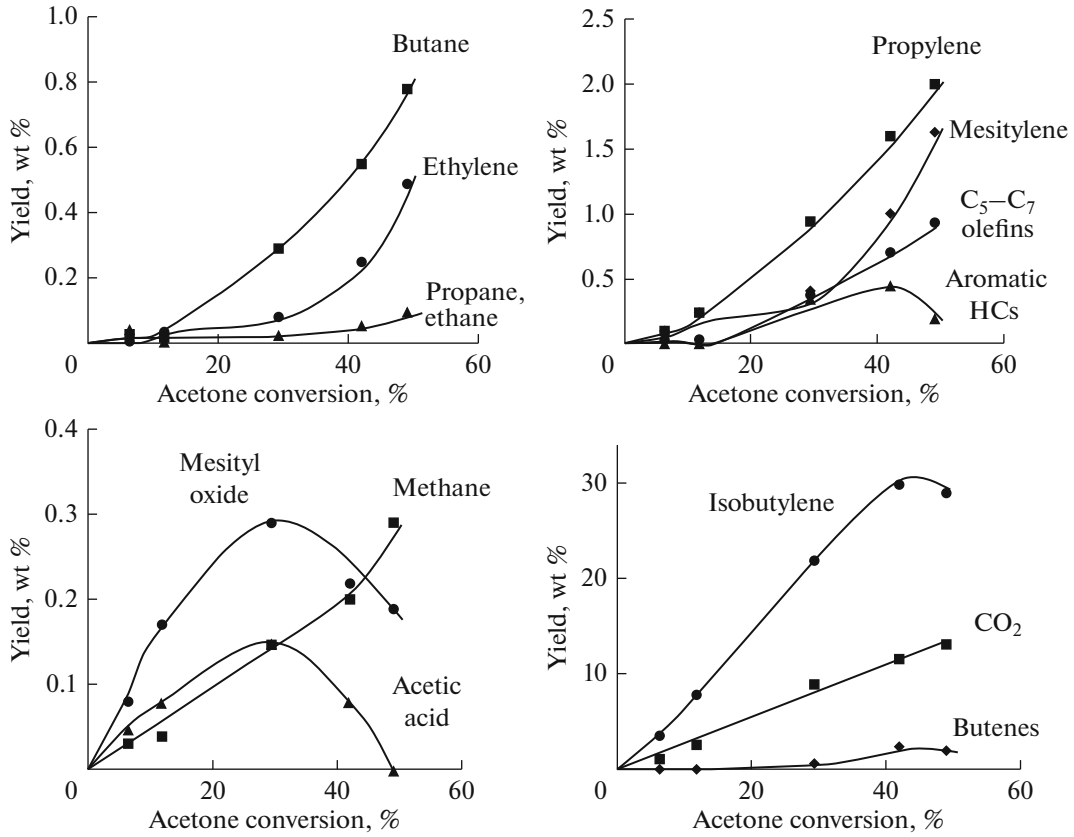

Fig. 3. Dependence of the product yield on acetone conversion in the presence of the MgRM-2 catalyst at 500°C.

was not observed in the reaction products, apparently, because of the high reactivity of this alcohol. It can be further converted either to isobutylene and acetic acid or to mesityl oxide—pseudoprimary products—owing to dehydration. Isobutylene is an unstable product: owing to the occurrence of oligomerization and cracking reactions, it is converted to aliphatic HCs. Acetic acid and mesityl oxide are also unstable products: acetic acid can undergo decomposition to form carbon dioxide, acetone, and water or be converted to methane and carbon dioxide. Apparently, under these conditions, the process occurs so rapidly that, at an acetone conversion of 3–5%, carbon dioxide is a primary product. There can be another route providing the formation of carbon dioxide as a primary product from acetone; additional studies in the low conversion region are required for a more reliable determination of whether CO_2 is a primary or secondary product. Methane, as a primary product, can be formed in acetone pyrolysis, which also leads to the formation of ketene, which is an extremely unstable product that can be converted to coke. The condensation of three acetone molecules, with subsequent dehydration and cyclization, leads to the formation of mesitylene and mesitylene isomers, which can undergo cracking to form other aromatic HCs. The dependence of yield on conversion for mesitylene has a shape characteristic of the sum of primary and secondary products; in addition, it is evident that the curve for other aromatic HCs passes through a maximum. Apparently, at higher conversions, mesitylene becomes dominant as a thermodynamically more stable product. The occurrence of many secondary conversions—apparently, metath-

Table 2. Classification of the products of catalytic acetone conversion

Product name	Product type
Isobutylene	Primary, unstable
Acetic acid	Primary, unstable
Methane	Primary + secondary, stable
Ethylene	Secondary, stable
Propylene	Secondary, stable
Butane	Secondary, stable
Butenes	Secondary, unstable
C_5–C_7	Secondary, stable
Mesityl oxide	Primary, unstable
Mesitylene	Primary + secondary, stable
Aromatic HCs	Secondary, unstable
Carbon dioxide	Primary, stable

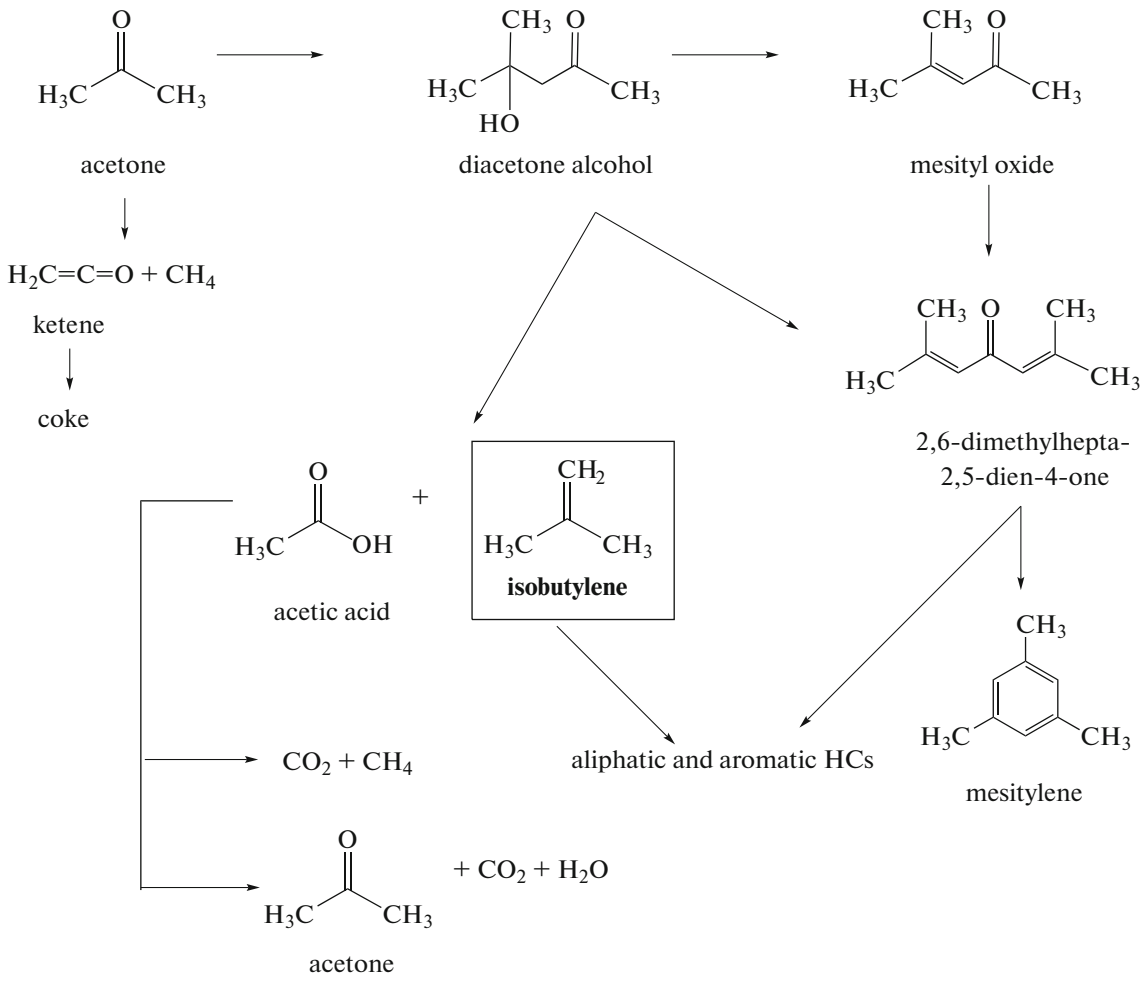

Fig. 4. Schematic catalytic conversion of acetone.

esis and hydrogen redistribution reactions—leads to the formation of C_2–C_7 alkanes and alkenes. In general, our results are consistent with the kinetic studies described in the literature [2, 12]; however, it should be noted that the authors of those studies did not take into account the formation of oxygen-containing products and carbon oxides.

Comparison of the catalytic properties of the Mg-containing catalysts based on MOR and the micro–mesoporous materials was conducted according to the initial rates of acetone conversion and target product—isobutylene—formation (Fig. 5). Upon switching from MgMOR to MgRM-3, the catalyst activity increases. Since the total number and strength of acid sites decrease in this order, the increase in the initial rate of acetone conversion is apparently attributed to the pore characteristics of the material. In fact, an increase in the degree of recrystallization leads to an increase in the pore volume, which facilitates the diffusion of molecules and makes the active sites of the catalyst more accessible. In addition, an increase in the initial rate of isobutylene formation with an increase in the mesopore content in the magnesium-modified samples suggests that isobutylene formation occurs on both Brønsted and Lewis acid sites, because, according to IR spectroscopy of adsorbed Py, an increase in the degree of recrystallization leads to a decrease in the number of Brønsted sites and an increase in the number of Lewis sites (Fig. 2).

Magnesium modification leads to the formation of a large number of new Lewis acid sites, as evidenced by the NH_3 TPD results (Table 1, Fig. 1) and the IR spectra of adsorbed Py (Fig. 2). However, comparison of the initial activities for MOR and MgMOR shows that this significant change in acidity does not lead to an increase in the catalyst activity (Fig. 5). Apparently, Lewis acid sites attributed to the presence of $Mg(OH)^+$ cations are not active in the reaction.

Table 3 lists selectivity values for the products of acetone conversion in the presence of Mg-containing MOR and micro–mesoporous catalysts at close acetone conversions. The amount of produced isobutylene increases in a row from MgMOR to MgRM-3. In this case, the amount of methane, ethylene, and pro-

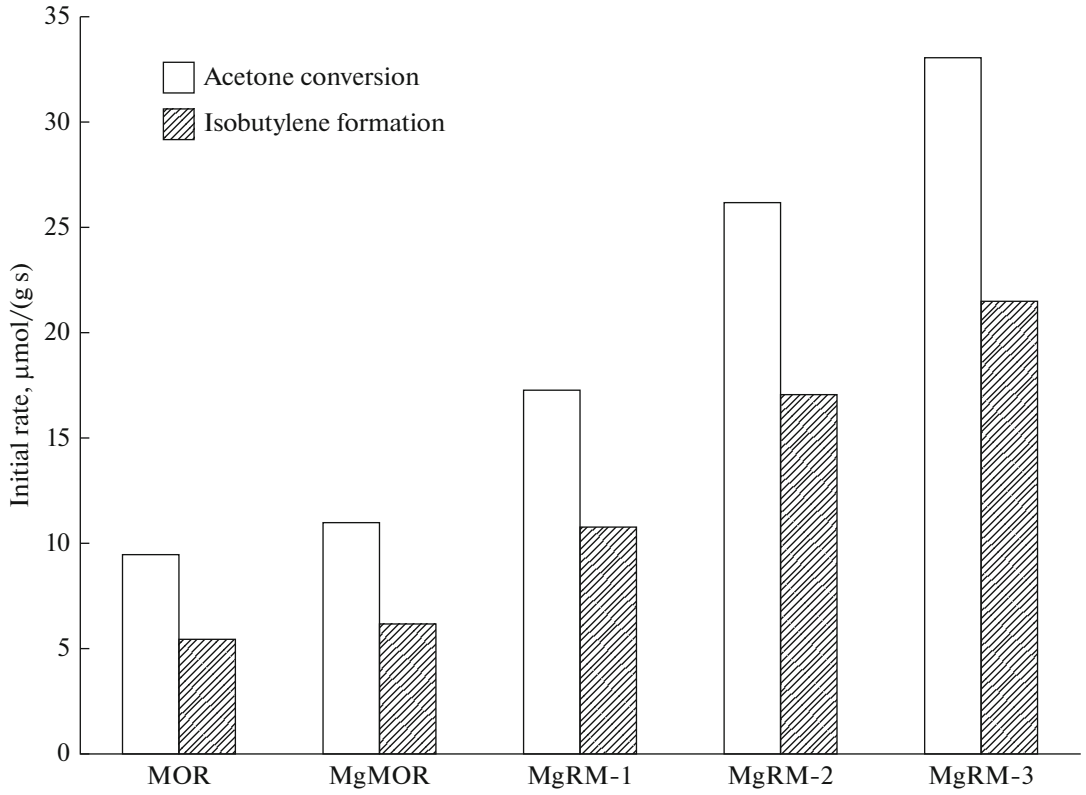

Fig. 5. Initial rates of acetone conversion and target isobutylene formation in the presence of the unmodified and magnesium-containing catalysts at 500°C and a WHSV of 72 h^{-1}.

pylene (secondary products) decreases in accordance with the proposed conversion scheme, while the amount of unstable products, such as acetic acid and mesityl oxide, increases.

Taking into account the acidic and pore characteristics of the catalysts, it can be concluded that the presence of strong Brønsted acid sites (as in MOR and weakly recrystallized material RM-1) is responsible

Table 3. Acetone conversion and selectivity towards reaction products in the presence of magnesium-modified MOR and micro–mesoporous catalysts at 500°C and 72 h^{-1}

Catalyst	MOR, 3%Mg	RM-1, 3%Mg	RM-2, 3%Mg	RM-3, 3%Mg
Conversion, %	3	5	7	8
Isobutylene	57.5	62.3	65.2	65.2
		Selectivity, mol %		
Methane	3.7	2.2	1.9	1.0
Ethylene	5.9	2.2	0.2	0.2
Ethane	0.3	0.0	0.0	0.0
CO_2	21.2	21.6	21.3	23.6
Propylene	8.1	4.9	3.0	1.7
Propane	0.0	0.0	0.0	0.0
C_4	0.7	2.5	1.4	0.3
C_5–C_7	0.1	1.8	1.0	1.5
Aromatic HCs	0.6	0.9	1.2	1.9
Acetic acid	0.4	0.8	3.5	2.9
Mesityl oxide	0.1	0.7	0.9	1.2

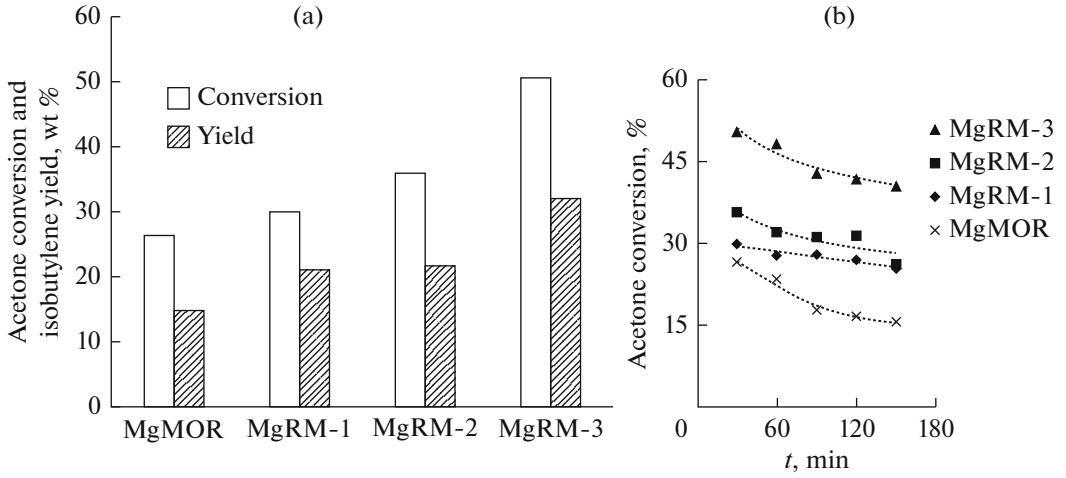

Fig. 6. (a) Isobutylene yield in the presence of different catalysts after 30 min of reaction and (b) time dependence of acetone conversion for the MgMOR–MgRM-3 set of magnesium-containing samples at 500°C and WHSV of 2 h^{-1}.

for the occurrence of undesirable secondary processes; the target product—isobutylene—apparently undergoes further conversions to form lower olefins. Therefore, in the presence of MOR and RM-1, the isobutylene selectivity is lower and the amount of light olefins is larger. With an increase in the degree of recrystallization, the number of strong Brønsted acid sites decreases. The RM-3 material mostly contains Lewis acid sites; their total number is sufficient for the occurrence of acetone conversion to isobutylene; in this case, the contribution of secondary processes is lower, as evidenced by a decrease in the amount of light olefins and the presence of unstable primary products, such as acetic acid and mesityl oxide. An increase in the amount of aromatic HCs upon switching from MOR to mesoporous RM-3 can be attributed to an increase in the pore size, i.e., an improvement in the transport characteristics of the catalyst.

Based on the results, it is possible to make an assumption on acetic acid conversion routes. Apparently, on strong Brønsted acid sites, acetic acid is converted to methane and carbon dioxide; with an increase in the amount of Lewis acid sites, another route—formation of acetone, water, and carbon dioxide—becomes dominant. Therefore, the products formed in the presence of MOR contain a larger amount of methane.

Comparison of the activity and on-stream stability of the Mg-containing catalysts was conducted at a feed WHSV of 2 h^{-1}; the results are shown in Fig. 6. In the MgMOR–MgRM-3 set of magnesium-modified samples, the acetone conversion varied from 26 to 52%, while the isobutylene selectivity varied only slightly (from 55 to 60 wt %); therefore, the target product yield was determined by acetone conversion. All the catalysts underwent deactivation over time, whereas the isobutylene selectivity hardly changed over time. The micro–mesoporous materials exhibit a more stable on-stream behavior than that of the original MOR sample. The significant deactivation of MgMOR can be caused by both the presence of strong Brønsted acid sites, which actively mediate coke formation processes, and the small size of the pores blocked by condensation products. Thus, the role of metal cations is to decrease the number of strong acid sites that mediate undesirable side reactions, in particular, coke formation, which leads to catalyst deactivation.

CONCLUSIONS

Thus, an increase in the mesopore content leads to an increase in the accessibility of active sites, facilitates the transport of feed reactants and reaction products, and thereby contributes to an increase in the activity of the catalysts in acetone conversion to isobutylene. An increase in the degree of recrystallization provides a decrease in the total amount of acid sites and an increase in the number of Lewis acid sites. According to the kinetic analysis of acetone conversion to isobutylene, it has been found that the main routes of acetone conversion are as follows: (1) aldol condensation to form diacetone alcohol, which further undergoes decomposition to form isobutylene and acetic acid; (2) the condensation of three acetone molecules with subsequent dehydration and cyclization to form mesitylene; and (3) the conversion of acetone condensation products to aliphatic and aromatic HCs. An increase in the mesopore content in the original zeolite leads to an increase in the catalyst activity owing to the removal of diffusion restrictions. Magnesium modification leads to a decrease in the number of strong Brønsted acid sites that mediate undesirable side reactions, in particular, coke formation, which leads to catalyst deactivation.

FUNDING

This work (synthesis of materials and analysis of their acidic properties) was supported by the Russian Science Foundation, project no. 19-73-10160.

REFERENCES

1. A. J. Cruz-Cabeka, D. Escuivel, C. Jimenez-Sanchidrian, and F. J. Romero-Salgnero, Materials **5**, 121 (2012).
2. T. Tago, H. Konno, M. Sakamoto, et al., Appl. Catal., A **403**, 183 (2011).
3. G. J. Hutchings, P. Johnston, D. F. Lee, et al., J. Catal. **147**, 177 (1994).
4. G. J. Hutchings, P. Johnston, D. F. Lee, and C. D. Williams, Catal. Lett. **21**, 49 (1993).
5. M. Nakai, K. Miyake, R. Inoue, et al., Microporous Mesoporous Mater. **273**, 189 (2019).
6. S. Hermann and E. Iglesia, J. Catal. **360**, 66 (2018).
7. L. Kubelkova and J. Novakova, Zeolites **11**, 822 (1991).
8. O. Kikhtyanin, V. Kelbichova, D. Vitvarova, et al., Catal. Today ***227***, 154 (2014).
9. C. D. Chang and A. J. Silvestri, J. Catal. **47**, 249 (1977).
10. S. Slamet and M. Nasikin, Int. J. Eng. Technol. **11**, 72 (2011).
11. J. Cejka and P. Jiru, Collect. Czech. Chem. Commun. **54**, 2998 (1989).
12. L. D. Dellon, C.-Y. Sung, D. J. Robichaud, and L. J. Broadbelt, Ind. Eng. Chem. Res. **58**, 15173 (2019).
13. C. Veloso, J. Monteiro, and E. Sousa-Aguiar, *Studies in Surface Science and Catalysis*, vol. 84: *Zeolites and Related Microporous Materials: State of the Art 1994*, Ed. by J. Weitkamp, H. G. Karge. H. Pfeifer, and W. Hölderich (Elsevier, Amsterdam, 1994), p. 1913.
14. O. A. Ponomareva, A. A. Maltseva, A. A. Maerle, et al., Pet. Chem. **56**, 253 (2016).
15. Y. Hirota, Y. Nakano, K. Watanabe, et al., Catal. Lett. **142**, 464 (2012).
16. G. S. Salvapati, K. V. Ramanamurty, and M. Janardanaro, J. Mol. Catal. **54**, 9 (1989).
17. A. N. Shuikin, L. G. Liberov, R. A. Fridman, et al., Neftekhimiya **17**, 715 (1977).
18. M. Demorest, D. Mooberry, and J. D. Danforth, Ind. Eng. Chem. **43**, 2569 (1951).
19. A. J. Crisci, H. Dou, T. Prasomsri, and Y. Roman-Leshkov, ACS Catal. **4**, 4196 (2014).
20. J. Sun, R. A. L. Baylon, C. Liu, et al., J. Am. Chem. Soc. **138**, 507 (2016).
21. H. Li, J. Sun, and Y. Wang, Appl. Catal., A **573**, 22 (2019).
22. M. Huang, P. A. Zielinski, J. Moulod, and S. Kaliaguine, Appl. Catal., A **118**, 33 (1994).
23. X. Long, Q. Zhang, Zh.-T. Liu, et al., Appl. Catal., B **134–135**, 381 (2013).
24. X. Guo, J. Shen, L. Sun, et al., Appl. Catal., A **261**, 183 (2004).
25. D. Mao, W. Yang, J. Xia, et al., J. Catal. **230**, 140 (2005).
26. I. I. Ivanova and E. E. Knyazeva, Chem. Soc. Rev. **42**, 3671 (2013).
27. I. A. Kasyanov, A. A. Maerle, I. I. Ivanova, and V. I. Zaikovskii, J. Mater. Chem., A **2**, 16978 (2014).
28. M. Tamura, K. Shimizu, and A. Satsuma, Appl. Catal., A **433–434**, 135 (2012).

Translated by M. Timoshinina